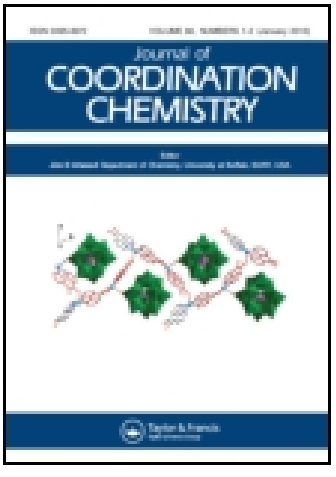

Journal of Coordination Chemistry
Publication details, including instructions for authors and subscription information:
http://www.tandfonline.com/loi/gcoo20

Antibacterial photoactivity and photosensitized oxidation of phenols with meso-tetra-(4-benzoate, 9-phenanthryl)-porphyrin and its metal complexes (Zn and Cu)

Olycen Oviedo[ab], Tamara Zoltan[a], Franklin Vargas[a], Marcel Inojosa[a] & Julio C. Vivas[a]

[a] Photochemistry Laboratory, Chemical Center, Venezuelan Institute for Scientific Research (IVIC), Caracas, Venezuela

[b] Faculty of Science, Department of Chemistry, University of Los Andes, Mérida, Venezuela

Published online: 22 May 2014.

To cite this article: Olycen Oviedo, Tamara Zoltan, Franklin Vargas, Marcel Inojosa & Julio C. Vivas (2014) Antibacterial photoactivity and photosensitized oxidation of phenols with meso-tetra-(4-benzoate, 9-phenanthryl)-porphyrin and its metal complexes (Zn and Cu), Journal of Coordination Chemistry, 67:10, 1715-1730, DOI: 10.1080/00958972.2014.917633

To link to this article: http://dx.doi.org/10.1080/00958972.2014.917633

Journal of Coordination Chemistry, 2014
Vol. 67, No. 10, 1715–1730, http://dx.doi.org/10.1080/00958972.2014.917633

Antibacterial photoactivity and photosensitized oxidation of phenols with *meso*-tetra-(4-benzoate, 9-phenanthryl)-porphyrin and its metal complexes (Zn and Cu)

OLYCEN OVIEDO†‡, TAMARA ZOLTAN*†, FRANKLIN VARGAS†, MARCEL INOJOSA† and JULIO C. VIVAS†

†Photochemistry Laboratory, Chemical Center, Venezuelan Institute for Scientific Research (IVIC), Caracas, Venezuela
‡Faculty of Science, Department of Chemistry, University of Los Andes, Mérida, Venezuela

(*Received 14 February 2014; accepted 27 March 2014*)

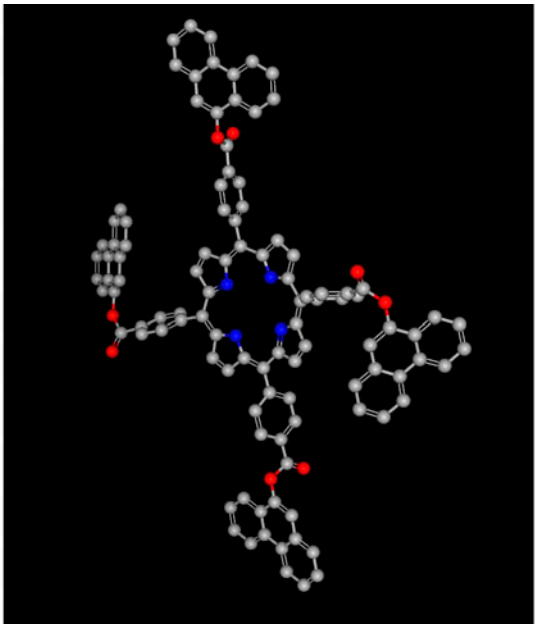

We performed the synthesis and characterization of *meso*-tetra-(4-benzoate-9-phenanthryl)-porphyrin and its Zn and Cu complexes. Synthesis of *meso*-tetra-(4-benzoate-9-phenanthryl)-porphyrin was carried out by dry gaseous HCl, *meso*-tetra-(4-carboxyphenyl)-porphyrin, and 9-phenantrol in tetrahydrofuran. The preparation of metal complexes was carried out using the method of the acetates. All porphyrins were characterized by FT-IR, NMR (^{1}H and ^{13}C), MS, UV–visible, and fluorescence spectroscopy. Their photophysical properties: photostability, fluorescence quantum yields, energy transfer, and generation of singlet oxygen were determined and compared with the *meso*-tetraphenyl

*Corresponding author. Email: tzoltan@ivic.gob.ve

porphyrin. Photochemical studies on their effectiveness as photosensitizers were performed through photo-oxidation of alcohols, phenol, and 2-naphthol. Higher efficiency of degradation was obtained with photostable TB9FPCu. The antibacterial photoactivity assay was tested against *Escherichia coli* and its viability was measured by chemiluminescence. The highest inactivation levels were obtained by ester TB9FP and Zn complex. The properties of the photosensitizer and its efficiency vary as a result of modifying its structure. The results obtained show that the efficiency of a photosensitizer depends on multiple factors. Thus, we can say that the copper complex is efficient in degradation of alcohol, while the metal-free porphyrin is better for antibacterial applications.

Keywords: Porphyrin; Photosensitizer; Quantum yield; Photo-oxidation; Antibacterial activity

1. Introduction

Porphyrins and metalloporphyrins have been the subject of numerous experimental and theoretical studies due to their remarkable photochemical, electrochemical, and biochemical properties [1]. Synthesis and functionalization of porphyrins have long been of interest because of the potential of porphyrin derivatives in diverse fields [2–11]. Substitution on the periphery of porphyrin rings of suitable organic groups as well as coordination of metal in the center of the porphyrin ring permits the design of new synthetic porphyrins. These modifications play a key role in the chemical, electronic absorption, and emission spectra, as well as redox properties [12]. A variety of organic reactions using multiple substituents have been employed to improve the periphery of porphyrins. However, few studies are found for modification of porphyrins by esterification reactions [12]. Substitution at meso positions of highly aromatic and bulky groups, such as naphthyl, phenanthryl, or pyrenyl porphyrins, have been reported, providing an increase in the quantum yields of the formation of reactive oxygen species (ROS) [13, 14]. It has also been reported that substitutions in the meso positions distort the core porphyrin ring, which alters its aromatic character decreasing its efficiency as a photosensitizer [15]. Thus, the main objective of this work is the synthesis of photosensitizers with highly resonant groups without loss of structural integrity of the porphyrin ring.

Considering that the *meso*-tetra-(4-carboxyphenyl)-porphyrin (TCPP) is a rigid and symmetric porphyrin, highly resonant groups without compromising the central ring may be included. Thus, in this study, we describe the esterification of the carboxylic groups of TCPP with highly resonant groups (phenanthryl) and its metal complexes. Synthesis and characterization of three new synthetic porphyrins, *meso*-tetra-(4-benzoate-9-phenanthryl)-porphyrin (TB9FP, **1**), and its Zn and Cu metal complexes (TB9FPZn, **2** and TB9FPCu, **3**) (figure 1) were carried out as well as their photophysical characterizations.

The effect of peripheral substitution and metal coordination was studied through photochemical characterization. The effect on the quantum yield of singlet oxygen and fluorescence and photostability of modifications to the porphyrin were studied. In addition, **1–3** were studied both in the photosensitized oxidation of phenols and photoinduced antibacterial efficiency.

2. Materials and methods

2.1. *General aspect*

All analytical or HPLC grade solvents, *meso*-tetra-(4-carboxyphenyl)porphyrin (TCPP), 9-phenanthrol, $Zn(CH_3COO)_2$, $Cu(CH_3COO)_2$, and 9,10-diphenylanthracene (DPA) were purchased from Sigma-Aldrich and used without purification.

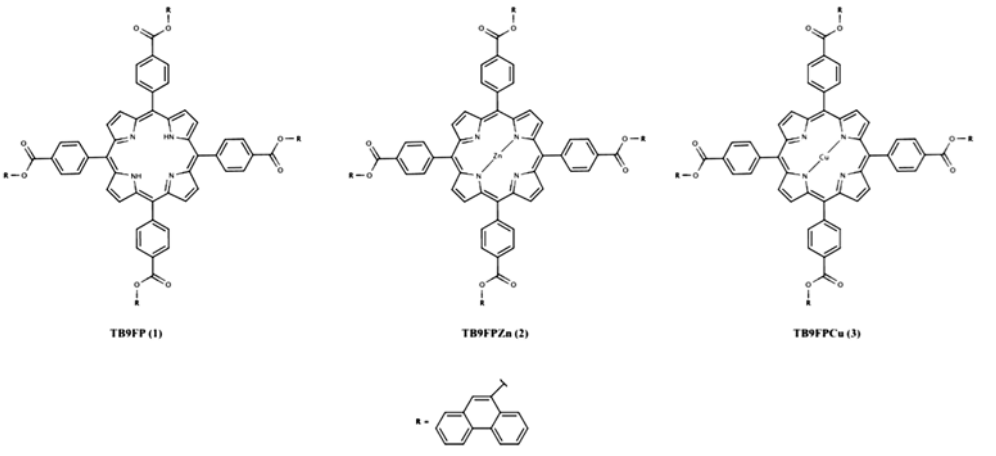

Figure 1. Structures of porphyrins used in this study: *meso*-tetra-(4-benzoate-9-phenanthryl)-porphyrin: (TB9FP, **1**); zinc *meso*-tetra-(4-benzoate-9-phenanthryl)-porphyrin: (TB9FPZn, **2**); and copper *meso*-tetra-(4-benzoate-9-phenanthryl)-porphyrin: (TB9FPCu, **3**).

^{1}H NMR and ^{13}C NMR spectra (figure 2) were recorded with a Bruker Avance 500 and 300 MHz, respectively, in chloroform-d with tetramethylsilane (Me_4Si) as an internal standard. Chemical shifts (δ) are given in parts per million. Infrared (IR) spectra were performed using a Nicolet Magna 560 FT-IR spectrometer. Electrospray ionization mass spectra and MS/MS spectra were obtained with a Thermo-Finnigan TSQ Quantum Ultra AM spectrometer coupled to a HPLC Electrospray. Elemental analyses were performed in a Fisons Instrument EA-1108. The samples were prepared by addition of the compound of interest to chloroform. Absorption spectra were recorded on a Perkin Elmer Lambda-35 UV–vis spectrophotometer. Fluorescence spectra and the quantum yields were registered in a Perkin Elmer LS-45.

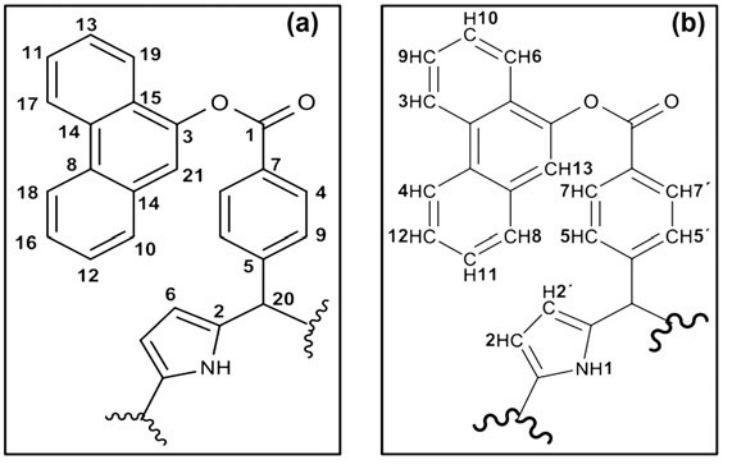

Figure 2. Assignment of signals ^{13}C NMR (a) and ^{1}H NMR (b) for TB9FP (**1**).

2.2. *Synthesis of the porphyrin derivatives*

2.2.1. Meso-tetra-(4-benzoate,9-phenanthryl)-porphyrin (TB9FP, 1). TB9FP (**1**) was synthesized (scheme 1) by adapting the procedure used by Vargas *et al.* [16]. The esterification was carried out by passing a stream of dry gaseous HCl through a solution of *meso*-tetra-(4-carboxyphenyl)porphyrin (TCPP, 201.3 mg, 0.255 mM) and 9-phenanthrol (497.0 mg, 2.56 mM) in THF (50 mL) without heating for five days. The reaction progress was followed by thin-layer chromatography and the crude product was separated and purified by column chromatography ($CHCl_3$/MeOH, 2 : 8). The purple crystals were washed with methanol. Yield: 41% (156.6 mg).

FT-IR (KBr, thin film) ν_{max} (cm^{-1}): 3435 (N–H), 3138–2853 (=C–H), 1744 (C=O), 1400 (C–N), 1384 (C–O–C), 1116 (C–O–C), 1102 (N–H), 802 (N–H), 617 (=C–H). MS: *m/z* 1293.80 $(M+H)^+$ Phenantrol (cal: 1292.41); 1496.53 $(M)^+$. Analysis, $C_{52}H_{31}N_2O_4$ calculated %C 69.065, %H 5.190, %N 1.870; found: %C 69.032, %H 5.236, %N 1.770. ^{1}H NMR (500 MHz, $CDCl_3$, δ, J = Hz): −2.808 (s, 4H, imino protons), 8.824 (s, 8H, pyrrols protons), 8.652 (d, J = 7.5, 4H, H3), 8.581 (d, J = 7.5, 4H, H4), 8.450 (d, J = 7.5, 4H, H5), 8.361 (d, J = 7.5, 4H, H6), 8.305 (d, J = 7.5, 4H, H7), 7.753 (d, J = 7.5, 4H, H8), 7.681 (t, J = 7.5, 4H, H9), 7.622 (t, J = 7.5, 4H, H10), 7.535 (t, J = 7.5, 4H, H11), 7.496 (t, J = 7.5, 4H, H12), 6.972 (s, 4H, H13). ^{13}C NMR (200 MHz, $CDCl_3$), δ = ppm: 166.688 (C=O, C1), 152.684 (C–N, C2), 146.721 (C–O, C3), 134.566 (C4), 132.910 (C5), 131.309 (C6), 129.879 (C7), 129.583 (C8), 128.003 (C9), 127.287 (C10), 127.160 (C11), 126.911 (C12), 126.610 (C13), 126.472 (C14), 126.400 (C15), 124.270 (C16), 122.566 (C17), 122.517 (C18), 122.499 (C19), 119.416 (C20), 102.649 (C21). UV–vis ($CHCl_3$), λ_{max} (nm): 420, 516, 550, 590, 648.

2.2.2. Zn-meso-tetra-(4-benzoate,9-phenanthryl)-porphyrin (TB9FPZn, 2) and Cu-meso-tetra-(4-benzoate,9-phenanthryl)-porphyrin (TB9FPCu, 3). Metallization of the TB9FP (**1**) was performed similarly for both products [17]: the dissolved ester (12.0 mg,

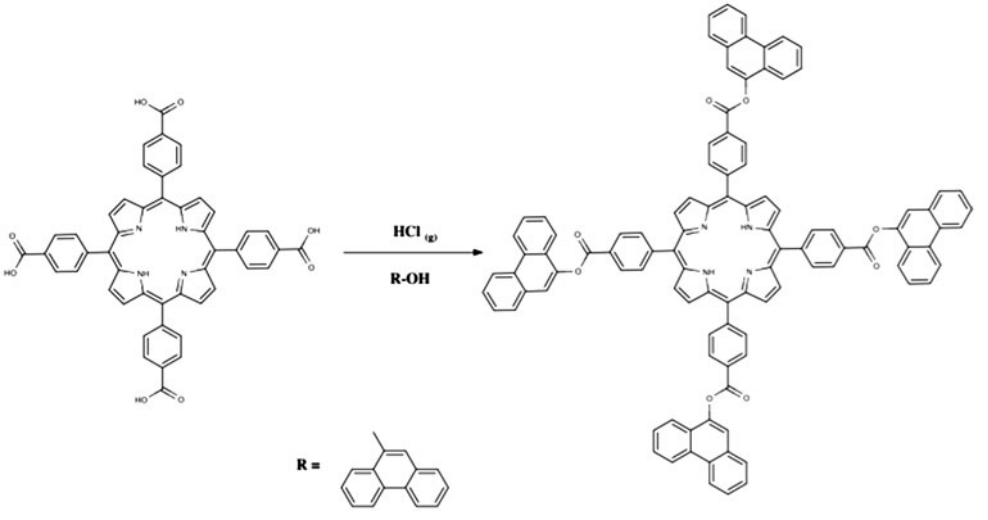

Scheme 1. Synthesis of *meso*-tetra-(4-benzoate-9-phenanthryl)-porphyrin: (TB9FP, **1**).

0.00802 mM) in chloroform with the corresponding metal acetate [$Cu(CH_3COO)_2$ 8.25 mg, 0.0413 mM; $Zn(CH_3COO)_2$ 9.10 mg, 0.0414 mM] was taken under constant stirring at room temperature. The metal coordination was followed by UV–visible spectroscopy and was stopped when there was no change in the absorption spectra in the Q band regions. The reaction mixture, in each case, was concentrated until dry. The solids obtained were washed with methanol to remove acetates. Yield of TB9FPZn (**2**) and TB9FPCu (**3**) was 89.74% and 72.83%, respectively.

2.2.2.1. *TB9FPZn (2).* FT-IR (KBr, thin film) ν_{max} (cm^{-1}): 3119.47 (=C–H), 2923.69–2853.14 (=C–H), 1731.33 (C=O), 1636.65 (C=C), 1384.54 (C–O–C), 1108.24 (C–O–C), 1102 (N–H), 617.91 (=C–H). UV–vis ($CHCl_3$), λ_{max} (nm): 421, 548, 631. The NMR (^1H and ^{13}C) spectra showed no significant changes in the observed signals except for the disappearance of the signal at −2 ppm as a result of the metallization.

2.2.2.2. *TB9FPCu (3).* FT-IR (KBr, thin film) ν_{max} (cm^{-1}): 3120.25 (=C–H), 2920.57–2850.79 (=C–H alquenos), 1717.34 (C=O), 1607.12 (C=C), 1384.48 (vta C–O–C), 1100.97 (C–O–C). UV–vis ($CHCl_3$), λ_{max} (nm): 417, 539, 675. The NMR (^1H and ^{13}C) spectra showed no significant changes in the observed signals except for the disappearance of the signal at −2 ppm as a result of the metallization.

2.3. *Irradiation*

All irradiations were carried out using a Rayonet photochemical reactor, consisting of a series of fluorescent lamps UV-A (320–400 nm, 3.3 mW cm^{-2}) and UV-B (280–320 nm, 3.3 mW cm^{-2}) along the cylindrical wall of the reactor surrounding the cell. The reactor has a fan to keep the sample at room temperature reducing thermal excitation of the solution.

2.4. *Photochemical characterization*

2.4.1. Photobleaching studies. Solutions of porphyrins **1–3** in $CHCl_3$ (1×10^{-5} M L^{-1}) were irradiated at room temperature in a Rayonet photochemical reactor at a distance of 10 cm between the lamp surface and the solution. The light emission was maximum for the photochemical reactor in UV-A 320–400 nm (3.3 mW cm^{-2}, 45.575 Lux seg^{-1}) and in UV-B (280–320 nm, 3.3 mW cm^{-2}), as measured with a UVX Digital Radiometer at 25 °C under oxygen. The course of the reaction was followed by UV–vis spectrophotometry using a Perkin Elmer Lambda-35 instrument. The absorbance spectra were recorded every 30 s for 10 min to observe the possible photobleaching by reduction of the photosensitizer concentration. The photostability was expressed as A_t/A_0 (A_t = absorbance of the Soret band at a given time of irradiation, A_0 = absorbance of the Soret band before irradiation).

2.4.2. Energy transfer. The efficiency of energy transfer from aromatic substituents towards the porphyrin ring was determined. Porphyrin derivatives 1–3 in $CHCl_3$ (1×10^{-5} M L^{-1}) were excited at the wavelength of the single substituent (9-phenantrol, λ_{exc}: 242 nm) obtaining the signal emission of the substituent 9-phenantrol (λ_{em}: 739 nm) inside the synthesized porphyrin derivative. Variations in the fluorescence spectra allow determining the energy transferred from the substituents to the porphyrin.

2.4.3. Fluorescence quantum yields. The relative fluorescence quantum yields for **1–3** were determined at room temperature by the comparative method using *meso*-tetraphenylporphyrin (TPP) as standard (1×10^{-5} M L^{-1} in $CHCl_3$; Φ_F 0.11 [18]). Fluorescence quantum yields (Φ_F) were determined using equation (1) [19],

$$\Phi_F = \Phi_F(\text{Std}) \frac{F A_{\text{Std}} \eta^2}{F_{\text{Std}} A \eta_{\text{Std}}^2} \tag{1}$$

where F and F_{Std} are the areas under the fluorescence curves of **1–3** and the standard, respectively, A and A_{Std} are the absorbances of the sample and standard at the excitation wavelengths, η and η_{Std} are the refractive indices of solvents used, respectively, for the sample and the standard.

2.4.4. Singlet oxygen generation. Singlet oxygen was measured by the DPA bleaching method [20]. The singlet oxygen with DPA reaction occurs with 100% chemical quenching (no competing physical quenching), and its disappearance kinetics can be followed by UV–vis spectrophotometry by gradually decreasing absorbance at 374 nm with respect to irradiation time (scheme 2) [20]. In a typical experiment, a DPA solution in chloroform (1.5 mL, 1×10^{-5} M L^{-1}) and porphyrin solution (1.5 mL, 1×10^{-5} M L^{-1}) in chloroform were placed in a quartz cuvette with a 1 cm optical path and irradiated with visible light (>420 nm) under oxygen and gentle magnetic stirring for different periods of time up to 20 min (2, 4, 6, 8, 10, 15, and 20 min).

Quantum yields of singlet oxygen photogeneration were determined in air (no oxygen bubbled) using the relative method with TPP as reference and DPA as a chemical quencher of singlet oxygen, from equation (2):

$$\Phi_\triangle = \Phi_\triangle(\text{Std}) \frac{W}{W^{\text{Std}}} \tag{2}$$

where Φ_Δ (Std) are the singlet oxygen quantum yields for the standard, TPP in chloroform being (0.50) [4], W and W^{Std} are the DPA photobleaching rates in the presence of the porphyrin complex and the standard, respectively [21].

2.5. *Photosensitized oxidation of aromatic alcohols*

The photodegradation assays were performed by the reaction of phenol and 2-naphthol with singlet oxygen generated by photosensitization to obtain 1,4-benzoquinone and 1,2-naphthoquinone, respectively (scheme 3) [22]. Photodegradation of phenol was carried out using

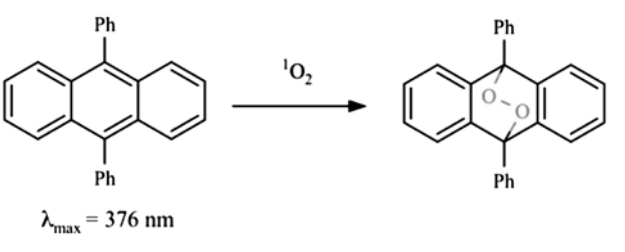

Scheme 2. Singlet oxygen oxidation of DPA to its endoperoxide.

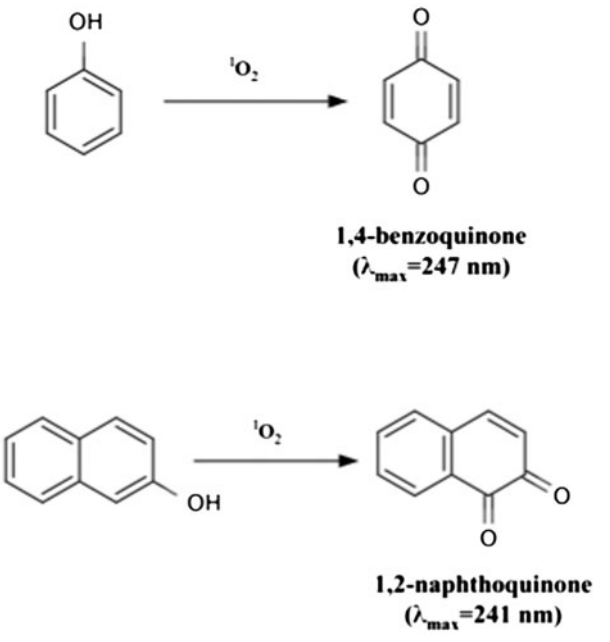

Scheme 3. Sensitized photo-oxidation reactions for phenol and 2-naphthol.

a molar ratio of 1 : 20 (porphyrins : alcohol) in chloroform. A mixture of alcohol and photosensitizer were irradiated with a Rayonet photochemical reactor, keeping 10 cm from lamp surface to sample solution, with an emission maximum in UV-A 320–400 nm (3.3 mW cm^2, 45.575 Lux seg^{-1}) for 45 min. The reaction was followed by the appearance of the corresponding band, 247 nm for 1,4-benzoquinone [22] and 241 nm for 1,2-naphthoquinone [23] in a Perkin Elmer Lambda-35 UV–vis spectrophotometer. Photodegradation efficiency of the sensitizers used was quantified by production yields of benzoquinone and naphthoquinone, based on the ideal performance assuming 100% of conversion.

2.6. *Antibacterial activity*

Antibacterial assays were carried out using *Escherichia coli* (ATCC 8739) and their proliferation and viability were obtained by chemiluminescence using BacTiter- Glo Microbial Cell (Promega, USA). Compounds **1–3** were prepared in H_2O : DMSO : Tween-80 : NaCl (95.16 : 4.0 : 0.04 : 0.8) in a concentration range of 1.0×10^{-6} to 5.0×10^{-6} M L^{-1}. We took into account that different bacteria have diverse amounts of ATP per cell, and values reported of ATP level in cells vary considerably. Factors that affect the ATP content of cells, such as growth phase, culture medium, and presence of metabolic inhibitors, can influence the relationship between cell concentration and luminescence. The antibacterial photoactivities were carried out under irradiation with an illuminator LuzChem LZC 4 V Photoreactor using 14 lamps with emission in UV-A (320–400 nm, 3.3 mW cm^{-2}, 45.575 Lux seg^{-1}), keeping 10 cm between the lamp surface and the solution flask, varying the time periods of exposure at 37 °C under continuous shaking.

The BacTiter-Glo Microbial Cell Viability Assay is a homogeneous method to determine the number of viable bacterial cells in a culture based on quantification of ATP present. ATP is an indicator of metabolically active cells. The homogeneous assay procedure involves adding a single reagent (BacTiter-Glo Reagent) directly to the bacterial cells in LB broth and measuring the luminescence. The luminescent signal is relative to the amount of ATP present, which is directly proportional to the number of living cells in the culture.

The recorded luminescence signals (Luminescence (RLU.): relative light units) represent the mean of three replicates for each measurement. The signal-to-noise ratio was calculated: S : N = [mean of signal × mean of background]/standard deviation of background.

A direct relationship (linear correlation) exists between luminescence measured with the BacTiter-Glo Microbial Cell Viability Assay and the number of cells in culture over five orders of magnitude. Values represent the mean ± SD of four replicates for each cell number. The luminescent signal from 50 *E. coli* cells is greater than three standard deviations above the background signal resulting from serum-supplemented medium without cells. There is a linear relationship ($r^2 = 0.99$) between the luminescent signal and the number of cells from 0 to 50,000 cells per well.

2.7. *Statistical treatment of results*

In each test, at least three independent experiments were performed unless stated otherwise. The figures show either single representative results or means (± SD where appropriate).

3. Results and discussion

3.1. *Primary photophysical properties of 1–3*

The fundamental step of any photochemical process is to absorb a photon by a photoexcitable molecule. In this way, absorption spectra describe the regions of the UV–visible, where these compounds absorb and hence are excited to higher energy states providing important data for characterization of the photosensitizer. Spectrophotometric studies of **1–3** were carried out using known concentrations in chloroform.

Absorption spectra of **1–3** show the typical porphyrins Soret band near 400 nm and four Q bands in the visible region. A band near 250 nm is associated with electronic transitions of phenanthryl. Absorption maxima and absorption coefficients of the sensitizers are presented in table 1, along with wavelengths of excitation and emission for each.

A small red shift was observed in the Soret band of **1** regarding TCPP, which could be attributed to a slight loss of planarity of the macrocycle due to the peripheral substituents [15]. The UV–vis spectra of metal complexes (table 1) all show the characteristic Soret band maxima and the corresponding displacement with respect to free base. This displacement is an indication of metal complexes with metals of configuration d^6–d^{10} [1]. Both metal complexes show a red shift, characteristic of structural deformation as a result of metal coordination on the porphyrin ring [24]. The number of Q bands is reduced to two, in line with the expected $D_{4\,h}$ symmetry.

By comparing UV–vis spectra (table 1) of the porphyrin complex of zinc (**2**) with copper porphyrin complex (**3**), a blue shift of the spectral bands of the copper complex is shown. As described by Gouterman [25], these blue shifts of the Soret and Q bands are attributed to strong effects of conjugation between Cu(II) orbitals and the π electrons of the tetrapyrrole

Table 1. Absorption spectra of porphyrins **1–3** in chloroform (1×10^{-5} M L^{-1}).

Porphyrin	Soret band, nm ($\varepsilon \times 10^4$ L M^{-1} cm^{-1})	Q Bands (nm)	λ_{exc} (nm)	λ_{em} (nm)
TCPP*	415.36 (105.9)	513.50 535.77 548.50 647.03	415.37	650.00
TB9FP (**1**)	420.84 (6.30)	516.00 550.96 590.90 648.57	417.90	650.38
TB9FPZn (**2**)	421.89 (3.27)	548.89 630.99	419.50	597.90
TB9FPCu (**3**)	417.54 (1.89)	539.05 675.82	422.00	656.29

*1×10^{-7} M L^{-1} in MeOH.

ring. These effects of conjugation cause a decrease in the energy of orbitals a_{1u} (π) and a_{2u} (π) relative to the orbitals e_g (π^*) and consequently an increase in the energy available for the electronic transitions [25].

Table 1 shows that in all cases, the fluorescence excitation spectrum coincides with the Soret band in the absorption spectrum, confirming that the excitation is associated directly with the energy absorption process. Furthermore, the wavelength of the fluorescent emission for **1** compared with TCPP indicates that inclusion of the aromatic groups has no effect on radiant deactivation processes. Likewise, if the metal coordination has an effect, a blue shift for Cu and red for Zn are observed.

3.1.1. Photobleaching studies. Energies and lifetimes of the excited states of the porphyrin complexes are dependent on the structure of the metal coordination complex and the nature of the solvent [26]. Substitutions in the macrocycle and metal ion at the center of the molecule give the greatest effects on stability of excited molecules. The photostability of the complexes is important to ensure the structural integrity of the complex when exposed to visible radiation and oxygen. In order to establish the rate of photodegradation of the compounds, we performed photostability studies under the same conditions as those used for the photooxidations and biological assay. Spectrophotometric studies carried out for estimating the photostability of **1–3** are shown in figure 3.

Figure 3 shows that the tendency of stability against UVA irradiation is TB9FPCu > TB9FPZn. This tendency is consistent with those reported by Fleischer [27] that describe the tendency of stability is directly associated with distance from the metal–nitrogen bond in metalloporphyrins, greater distance, less stability. The high stability observed in the copper complex can be explained due to the Cu–N bond of 1.98 Å, while the Zn–N bond distance is 2.05 Å, explaining the low stability against UVA irradiation. Thus, for TB9FPZn, UVA radiation is sufficiently strong to compromise its structural integrity, whereas for TB9FPCu integrity is not affected by radiation.

To explain the behavior of the Soret band for the free base (**1**) shown in figure 3, it is necessary to observe their behavior throughout the electromagnetic spectrum (figure 4). As irradiation time increases, the band at ~450 nm increases with simultaneous decrease in the Soret band at 420 nm. In addition, in the region between 500 and 700 nm, there is a decrease of the intensity of the four Q bands simultaneously with increase of two new

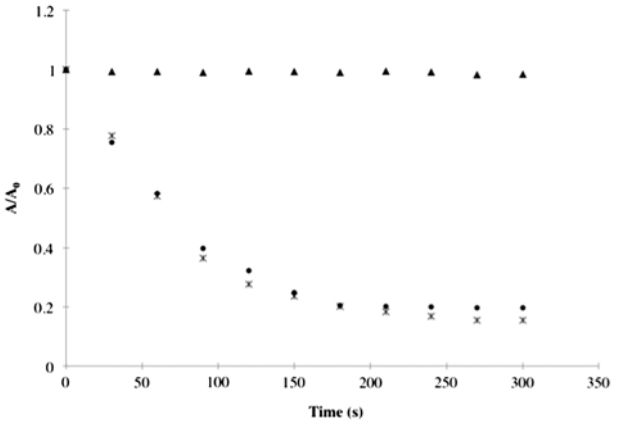

Figure 3. Porphyrin derivatives photobleaching at different irradiation times. The porphyrin bleaching was monitored by measuring the decrease of absorbance at the maximum of the Soret band: 421 nm TB9FP **1** (*, 422 nm TB9FPZn **2**) (* and 417 nm TB9FPCu **3** (▲)).

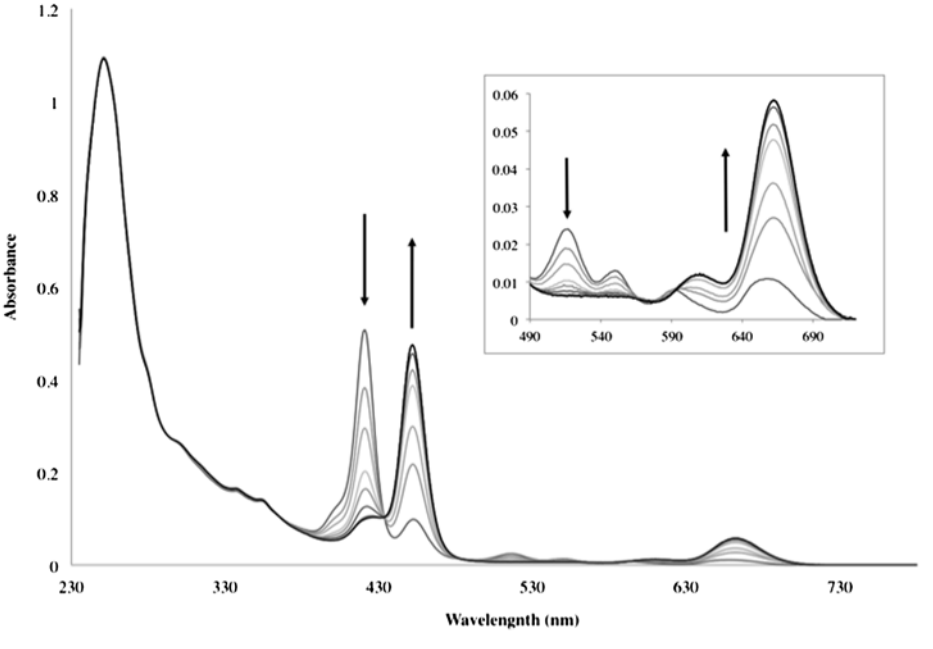

Figure 4. Spectral changes of TB9FP (**1**) upon UV-A irradiation at different times.

bands at ~548 and 647 nm. The changes observed in spectra of the free base can be attributed to protonation of nitrogen of pyrrole as the solvent effect [$H_2P_{(solv)} + H_2^{+}{}_{(solv)} \leftrightarrow H_4P_2^{+}{}_{(solv)}$]. Based on the proton donating ability of chloroform and similarity in metalloporphyrins, degeneration of the electronic levels is obtained with an increased molecular symmetry from D_{2h} to D_{4h} [28, 29] and a variation in the absorption spectrum between 500 and 700 nm.

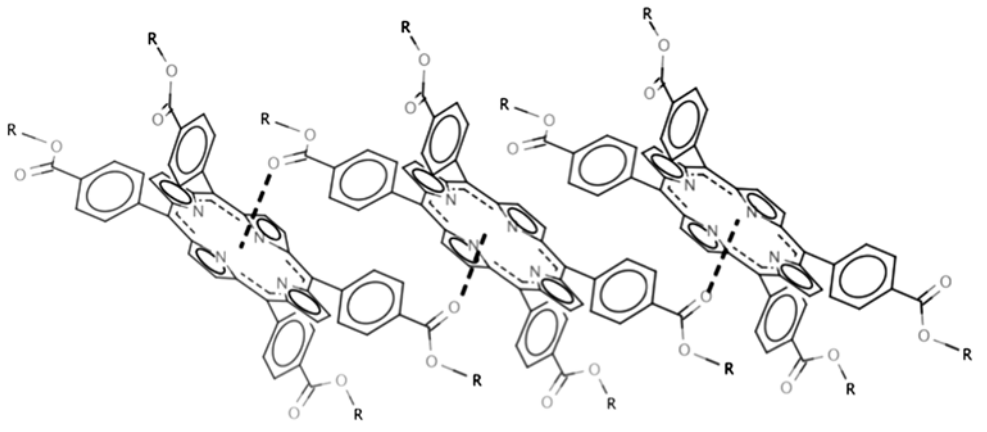

Figure 5. Proposed structure of the J-aggregates of **1**.

It has been reported that protonated form of the free base porphyrin in solution tends to form aggregates of type *H* and/or *J* [28, 29]. A shift of the Soret band UV spectrum indicates the presence of these aggregates. A bathochromic shift (blue shift) indicates side-by-side aggregates (*J*-aggregates) while a hypsochromic shift (red shift) indicates one type or face to face (*H*-aggregates). Given that the observed displacement in the Soret band is a red shift, it can be inferred that *J*-aggregates are formed, without compromising the integrity of the molecule. Figure 5 shows a graphical representation we have proposed for formation of aggregates for **1**.

3.1.2. Energy transfer. The porphyrins synthesized show an intensive red emission at 597–656 nm (table 1). Complexes **1–3** were excited at the maximum absorption wavelength of phenanthrene (251 nm), and the emission of porphyrin core was observed. The percent yields of energy transferred from the substituents to the porphyrin ring were TB9FP (**1**) 84.81%, TB9FPZn (**2**) 90.62%, and TB9FPCu (**3**) 96.94%. These results show a significant contribution to the energy of the fluorescence from phenanthryl groups in the compounds. Thus, highly aromatic groups allow efficient transfer of the stored energy.

3.2. *Fluorescence quantum yield*

The wide variety of applications of porphyrin derivatives is based on an ability of the complexes to generate ROS. A photosensitizer in its excited state can interact with triplet oxygen in the ground state to generate singlet oxygen [30], responsible for many of the photoinduced oxidative processes in applications of porphyrins. Fluorescence emission must be evaluated as a measure of energy transfer from the photoexcited sensitizer. Information about the efficiency of fluorescence emission as a route to deactivation is utilized when porphyrin compounds are used as tumor or cellular markers [31]. Therefore, the quantum yields were measured to evaluate the potential use of these new porphyrin derivatives as photosensitizers.

The values of fluorescence quantum yields (Φ_F) of **1–3** in chloroform are summarized in table 2. The fluorescence quantum yields were calculated using TPP as reference 0.110 [18].

From the values obtained for Φ_F, clearly there is a favorable effect on the fluorescence quantum yield of TABP ($\Phi_F = 0.010$) by including phenanthryl groups by esterification in **1** ($\Phi_F = 0.078$). In addition, the fluorescence quantum yield of the copper derivative (**3**, $\Phi_F = 0.063$) is greater than that obtained for the zinc derivative (**2**, $\Phi_F = 0.047$). Both metal derivatives show a fluorescence quantum yield lower than **1**. It has been reported [32] that metal coordination in porphyrins strongly affects the fluorescence by increasing the radiationless decay rate for intersystem crossing to the excited triplet state, resulting in a decrease in the fluorescence quantum yield.

3.3. *Singlet oxygen generation*

Singlet oxygen ($^1O_2$) is one of the ROS generated photochemically. To evaluate the photosensitizing efficacy of the porphyrins, the singlet oxygen quantum yields (Φ_Δ) were measured. TPP was used as the standard for determining Φ_Δ of the complexes, and the results are shown in table 3. Photogeneration of singlet oxygen of **1–3** (1×10^{-5} M L^{-1}) was studied and quantified indirectly using DPA as $^1O_2$ trapping with an irradiation time of 20 min (figure 6).

Figure 6 shows that production of singlet oxygen is increased by esterification: TB9FP > TBAP. Furthermore, both **2** and **3** show a singlet oxygen production lower than the free base resulting in a tendency for the production of singlet oxygen: **1** > **2** > **3**.

The efficiency of transfer of energy necessary for generation of singlet oxygen is dependent on the rate (or lifetime) of deactivating mechanisms of photoexcited molecules. Copper complex **3** is less efficient in the production of singlet oxygen. This phenomenon has been reported previously for other porphyrin complexes with paramagnetic metals [33]. This behavior is attributed to a non radiant relaxation given by the partially filled d orbitals of the metal to the porphyrin in the excited triplet state not allowing energy transfer to molecular oxygen. Complexes **1** and **2** exhibit a substantial $^1O_2$ quantum yield, which makes them excellent potential PDT agents.

Table 2. Relative quantum yields (Φ_F) of **1–3**.

Porphyrins	λ_{exc} (nm)	λ_{em} (nm)	Φ_F
TABP	415.37	650.00	0.010
TB9FP (**1**)	417.90	650.38	0.078
TB9FPZn (**2**)	419.50	597.90	0.047
TB9FPCu (**3**)	422.00	656.29	0.063

Table 3. Quantum yields (Φ_Δ) and quantification of singlet oxygen by **1–3** using the methodology of the degradation of DPA.

Porphyrins	Φ^1O_2	[$^1O_2$] M L^{-1}	M $^1O_2$/M Porphyrins
TABP	0.102	2.0×10^{-5}	2.00
TB9FP (**1**)	0.124	3.1×10^{-5}	3.10
TB9FPZn (**2**)	0.039	7.6×10^{-6}	0.76
TB9FPCu (**3**)	0.024	4.8×10^{-6}	0.48

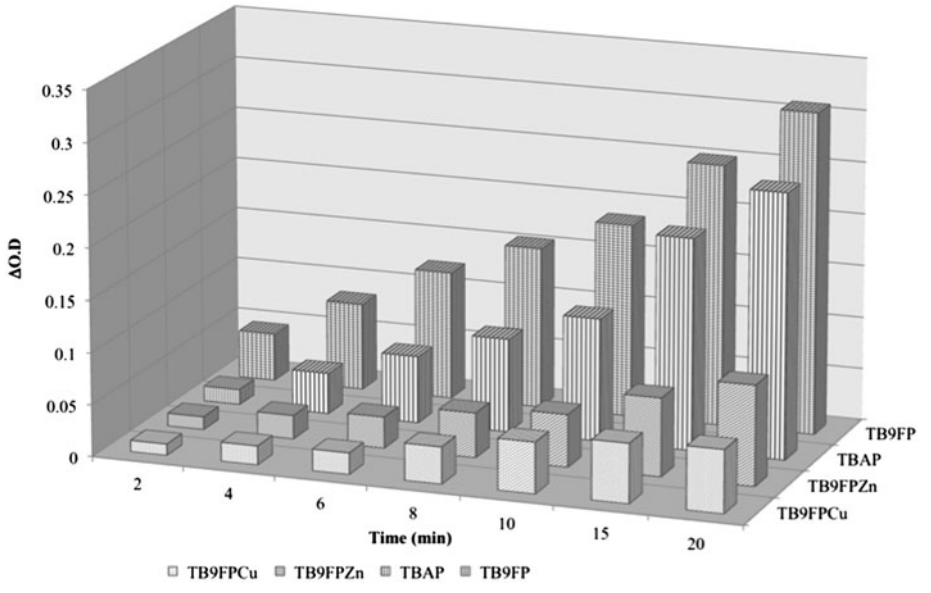

Figure 6. Effect of 20 min irradiation of **1–3** and TBAP on the bleaching of DPA at 374 nm. Δ_{OD} represents the difference in optical density of irradiated sample of **1–3** and TBAP.

3.4. *Photosensitized oxidation of aromatic alcohols*

The photo-oxidative properties of **1–3** were investigated in the same conditions. Photodegradation efficiencies of phenol (PN) and 2-naphthol (2-NP) were studied with **1**, **2,** and **3**, following changes in absorption spectra of both alcohols as a result of irradiation time. Initially, it was verified that NP or 2-NP will not degrade as a result of irradiation without porphyrins. The results obtained for degradation are shown in table 3.

These significant differences between the efficiencies in the degradation of the NP with free porphyrin and metalloporphyrins indicate the importance of the metal coordination in photodegradation mechanisms [34]. For the degradation of 2-PN, these differences are less marked. It has been reported that the efficiency of a photosensitizer is related to its stability and efficiency to produce ROS [35]. Thus, if we compare the stabilities of **2** and **3**, we see the high effectiveness for degradation of NP and 2PN by copper complex that can be explained according of their great photochemical stability, reported for heterogeneous systems [36].

A further important observation is that the trends in both degradations are inverse to quantum yields of singlet oxygen, which we can infer that these degradations involve other ROS like radicals, which have been reported to degrade efficiently this type of alcohol [37]. The low activity exhibited by **1** may be explained for aggregate formation that reduces the lifetime of the excited triplet state, making it inefficient on energy transfer and less efficient as a photosensitizer [38].

3.5. *Antibacterial activity*

Inactivation studies on *E. coli* (ATCC 8739) by **1**, **2,** and **3**, performed under UV-A (320–400 nm, 3.3 mW cm^{-2}, 45.575 Lux seg^{-1}), show that the complexes do not exhibit

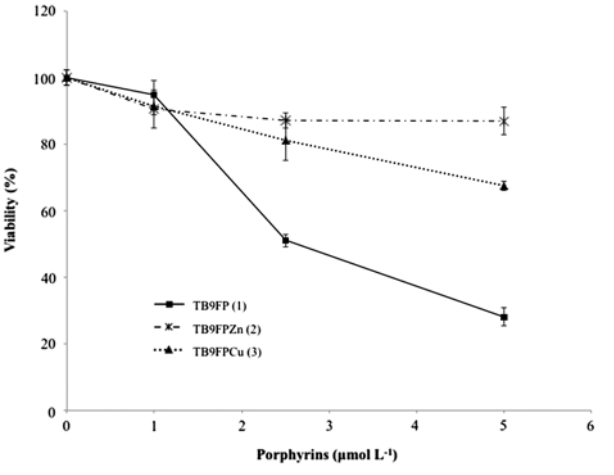

Figure 7. Cell viability assay (*E. coli*) in the presence of **1** (■), **2** (✳), and **3** (▲) at different concentrations. The result is based on quantification of the ATP present measured by luminescence after 15 min irradiation at each concentration.

Table 4. Yields of the phosensitized oxidation of phenol and 2-naphthol with $^1O_2$, after an hour of irradiation.

Porphyrins	Phenol degradation (%)	2-Naphthol degradation (%)	Φ^1O_2
TB9FP (**1**)	4.59	33.21	0.124
TB9FPZn (**2**)	7.13	33.90	0.039
TB9FPCu (**3**)	53.68	37.23	0.024

dark toxicity toward the bacteria at the tested concentrations (figure 7). Direct exposure of these bacterial strains to light, without synthetized complexes (light control), did not cause any cytotoxic effect.

Figure 7 shows comparative antibacterial action photoinduced only when **1–3** were irradiated for 15 min in the presence of *E. coli* at different concentrations. The compounds exhibit a photoinduced dose-dependent activity, with a tendency **1** > **3** > **2**, which does not coincide with the production of $^1O_2$ (table 4).

A *T* test for independent samples was carried out using the highest concentrations of porphyrin complexes, showing statistically significant differences at $p < 0.05$. The difference in activity obtained between Zn complex and the free base confirms that the main mechanism of bacterial photoinactivation is mediated by $^1O_2$ [39]. The activity obtained with the copper complex, despite its low quantum yield of singlet oxygen, can be explained by the production of other ROS, which are involved in the photoinduced antibacterial activity [40].

4. Conclusion

A porphyrin and metalloporphyrins TB9FP (**1**), TB9FPZn (**2**), and TB9FPCu (**3**) were synthesized and characterized, with high yield under mild reaction conditions. The

photochemical and photophysical characterization show the effect of substituent groups and the porphyrin metal centers in characteristics of new photosensitizers. The variations obtained in degradation of phenols, **3** > **2** > **1**, are directly related to the photochemical stability of photosensitizers and production of other ROS. Furthermore, the antibacterial activity, **1** > **3** > **2**, indicates that a synergy exists between the photochemical stability and singlet oxygen production in such activity. Thus, it was demonstrated that the stabilities of the photosensitizers and production of other ROS are responsible for efficiency of the synthesized complexes. Finally, of the three complexes, TB9FPCu (**3**) has the best features to be considered as an efficient photosensitizer.

References

[1] J.E. Falk. *Porphyrins and Metalloporphyrins*, Elsevier Scientific, Amsterdam (1975).
[2] G. Garcia, D. Naud-Martin, D. Carrez, A. Croisy, P. Maillard. *Tetrahedron*, **67**, 4924 (2011).
[3] Y.-C. Lim, J.-O. Yoo, S.-S. Kang, Y.-M. Kim, K.-S. Ha. *Cancer Sci.*, **102**, 549 (2011).
[4] A. Serra, M. Pineiro, A. Rocha Gonsalves, M. Abrantes, M. Laranjo, A. Santos, M. Botelho. *J. Photochem. Photobiol., B*, **92**, 59 (2008).
[5] C. Paul-Roth, G. Simonneaux. *C.R. Chim.*, **9**, 1277 (2006).
[6] A.R. Bhat, A.I. Bhat, F. Athar, A. Azam. *Helv. Chim. Acta*, **92**, 1644 (2009).
[7] M.P. Donzello, C. Ercolani, P.A. Stuzhin. *Coord. Chem. Rev.*, **250**, 1530 (2006).
[8] F. Figueira, J.A.S. Cavaleiro, J.P.C. Tomé. *J. Porphyrins Phthalocyanines*, **15**, 517 (2011).
[9] S.W. Park, D.S. Hwang, D.Y. Kim, D. Kim. *J. Chin. Chem. Soc.*, **57**, 1111 (2010).
[10] M. Trytek, M. Majdan, J. Fiedurek. In *Homogeneous and Heterogeneous Free-Based Porphyrins Incorporated to Silica Gel as Fluorescent Materials and Visible Light Catalysts Mimic Monooxygenases*, A. George (Ed.), Biomimetic Based Applications, pp. 59–104, InTech, Rijeka (2011).
[11] P.-C. Yao, S.-T. Hang, C.-W. Lin, D.-H. Hai. *J. Taiwan Inst. Chem. Eng.*, **42**, 470 (2011).
[12] W. Chen, S. Fukuzumi. *Eur. J. Inorg. Chem.*, **2009**, 5494 (2009).
[13] D. Murtinho, M. Pineiro, M.M. Pereira, A.M.d'A. Rocha Gonsalves, M. da Graça Miguel, H.D. Burrows. *J. Chem. Soc., Perkin Trans.* **2**, 2441 (2000).
[14] T. Zoltan, F. Vargas, C. Rivas, V. Lopez, J. Perez, A. Biassuto. *Sci. Pharm.*, **78**, 23 (2010).
[15] S. Zakavi, R. Omidyan, L. Ebrahimi, F. Heidarizadi. *Inorg. Chem. Commun.*, **14**, 1827 (2011).
[16] F. Vargas, T. Zoltan, C. Rivas, A. Ramirez, T. Cordero, Y. Díaz, C. Izzo, Y.M. Cárdenas, V. López, L. Gómez, J. Ortega, A. Fuentes. *J. Photochem. Photobiol. B*, **92**, 83 (2008).
[17] K.M. Smith, J.E. Falk. In *Porphyrins and Metalloporphyrins*, New ed./based on the original volume by J.E. Falk, K.M. Smith (Eds.), p. 798, Elsevier Scientific, New York (1975).
[18] H. Fonda, J. Gilbert, R. Cormier, J. Sprague, K. Kamioka, J. Connolly. *J. Phys. Chem.*, **97**, 7024 (1993).
[19] M. Durmuş, T. Nyokong. *Spectrochim. Acta Part A*, **69**, 1170 (2008).
[20] H.-Y. Lee, S. Chen, M.-H. Zhang, T. Shen. *J. Photochem. Photobiol. B*, **71**, 43 (2003).
[21] A. Ogunsipe, J. Chen, T. Nyokong. *New J. Chem.*, **28**, 822 (2004).
[22] S. Qourzal, N. Barka, M. Tamimi, A. Assabbane, Y. Ait-Ichou. *Appl. Catal., A*, **334**, 386 (2008).
[23] S. Nagakura, A. Kuboyama. *J. Am. Chem. Soc.*, **76**, 1003 (1954).
[24] W. Zheng, N. Shan, L. Yu, X. Wang. *Dyes Pigm.*, **77**, 153 (2008).
[25] M. Gouterman. In *The Porphyrins*, D. Dolphin (Ed.), pp. 1–165, Academic Press, New York (1978).
[26] T. Goslinski, T. Osmalek, K. Konopka, M. Wierzchowski, P. Fita, J. Mielcarek. *Polyhedron*, **30**, 1538 (2011).
[27] E.B. Fleischer. *Acc. Chem. Res.*, **3**, 105 (1970).
[28] D.B. Berezin. *Russ. J. Gen. Chem.*, **75**, 807 (2005).
[29] A. Rosa, G. Ricciardi, E.J. Baerends, A. Romeo, L.M. Scolaro. *J. Phys. Chem. A*, **107**, 11468 (2003).
[30] P. Agostinis, K. Berg, K.A. Cengel, T.H. Foster, A.W. Girotti, S.O. Gollnick, S.M. Hahn, M.R. Hamblin, A. Juzeniene, D. Kessel, M. Korbelik, J. Moan, P. Mroz, D. Nowis, J. Piette, B.C. Wilson, J. Golab. *CA. Cancer J. Clin.*, **61**, 250 (2011).
[31] A.E. O'Connor, M.M. Mc Gee, Y. Likar, V. Ponomarev, J.J. Callanan, D.F. O'Shea, A.T. Byrne, W.M. Gallagher. *Int. J. Cancer*, **130**, 705 (2012).
[32] T. Wijesekera, D. Dolphin. In *Methods in Porphyrin Photosensitization*, D. Kessel (Ed.), pp. 229–266, Methods in Porphyrin Photosensitization, Springer, New York (1985).
[33] K. Wang, C.-T. Poon, W.-K. Wong, W.-Y. Wong, C.Y. Choi, D.W.J. Kwong, H. Zhang, Z.-Y. Li. *Eur. J. Inorg. Chem.*, **2009**, 922 (2009).
[34] M. Hajimohammadi, N. Safari, H. Mofakham, F. Deyhimi. *Green Chem.*, **13**, 991 (2011).
[35] M. DeRosa, R. Crutchley. *Coord. Chem. Rev.*, **233–234**, 351 (2002).

[36] G. Vasapollo, G. Mele, R.D. Sole, I. Pio, J. Li, S.E. Mazzetto. *Molecules*, **16**, 5769 (2011).
[37] D. Zhang, R. Qiu, L. Song, B. Eric, Y. Mo, X. Huang. *J. Hazard. Mater.*, **163**, 843 (2009).
[38] Y.-T. Yang, C.-T. Chen, T. Tsai. *Dyes Pigm.*, **96**, 763 (2013).
[39] D.C. Costa, M.C. Gomes, M.A. Faustino, M.G. Neves, A. Cunha, J.A. Cavaleiro, A. Almeida, J.P. Tomé. *Photochem. Photobiol. Sci.*, **11**, 1905 (2012).
[40] K. Ergaieg, M. Chevanne, J. Cillard, R. Seux. *Solar Energy*, **82**, 1107 (2008).